Bioprocess and Biosystems Engineering (2019) 42:541–553
https://doi.org/10.1007/s00449-018-2057-2

RESEARCH PAPER

Valorization of mutant *Bacillus licheniformis* M09 supernatant for green synthesis of silver nanoparticles: photocatalytic dye degradation, antibacterial activity, and cytotoxicity

Bilal Momin[1] · Shakeelur Rahman[2] · Neetu Jha[2] · Uday S. Annapure[1]

Received: 10 November 2018 / Accepted: 7 December 2018 / Published online: 2 January 2019

Abstract
The present study reports the optimization of a green method for the synthesis of silver nanoparticles (AgNPs) via reduction of Ag^+ ions using cell-free supernatant of mutant *Bacillus licheniformis* M09. UV–Visible spectroscopy showing an absorption peak at ~ 430 nm confirmed the synthesis of AgNPs. Transmission electron microscope (TEM) analysis exhibited spherical AgNPs within the size range of 10–30 nm. Fourier transform infrared (FTIR) measurements assured the presence of effective functional molecules which could be responsible for stabilizing the AgNPs. X-ray diffraction (XRD) pattern verified the crystalline nature of AgNPs. Furthermore, the synthesized AgNPs showed an excellent photocatalytic degradation of methylene blue dye in less than 3 h under visible light proving their potential as a catalytic agent for bioremediation for next-generation dye degradation in effluent treatment. The AgNPs demonstrated antimicrobial activity against Gram-positive and Gram-negative foodborne pathogens which endorsed its suitability as agents to extend shelf-life in food packaging and food safety applications. The results also revealed a strong concentration-dependent cytotoxicity of AgNPs against human breast adenocarcinoma cells (MCF-7), while 15.07 µg/mL of IC_{50} was attained. The outcome suggests the possible application of these AgNPs in nanomedicine formulations. Thus, these findings propose promising ways for the valorization of the waste fermentation supernatant left after cell harvesting and desired metabolite extraction.

Extended author information available on the last page of the article

Graphical abstract

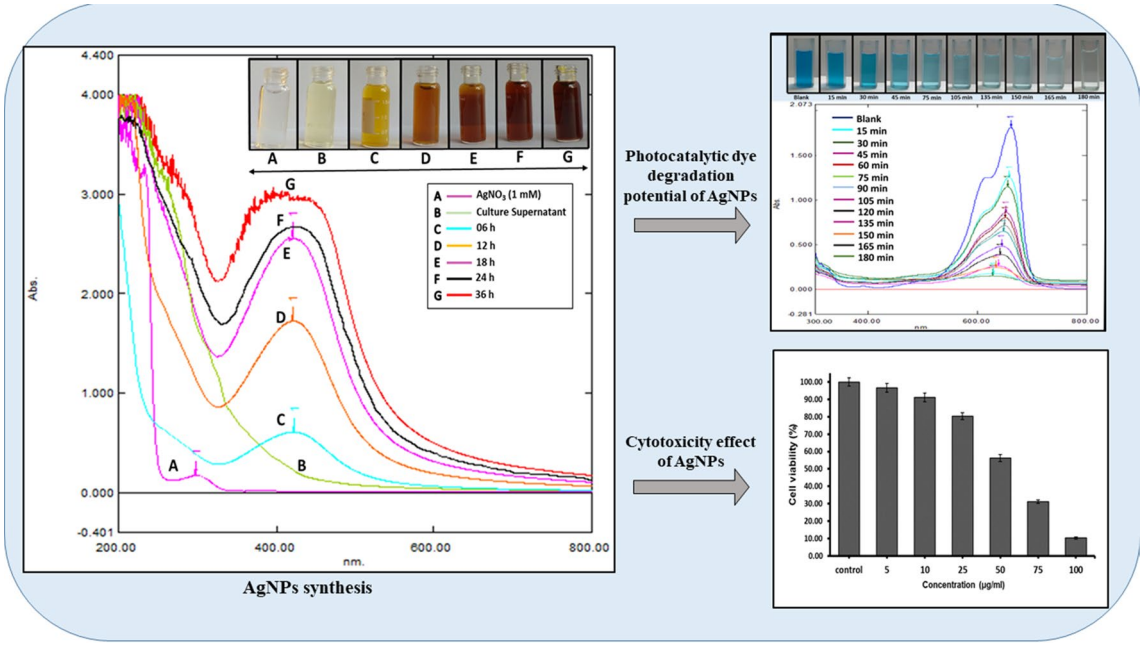

Keywords *Bacillus licheniformis* M09 · Silver nanoparticles · Methylene blue · Photocatalytic dye degradation · Antibacterial · Cytotoxicity effects

Introduction

In recent years, nanoparticles have found applications in diverse fields like electronics [1, 2], catalysis [3], biosensors [4], medicine, enzyme immobilization, and stabilization [5, 6], and energy [7] due to which their demand has increased progressively. The traditional techniques used for nanoparticles synthesis are expensive and time-consuming, and possess potential environmental and biological risks [8]. Hence, there is an ever-rising need for the development of an eco-friendly process to synthesize nanoparticles. Various biological approaches have been proposed for nanoparticle synthesis using enzymes, microorganisms, plants, and fungi [9, 10]. These are environmentally feasible, cost-effective, and time-efficient alternatives to the available chemical and physical methods.

Among various nanoparticles, silver nanoparticles (AgNPs) have gained tremendous importance as an antimicrobial, larvicidal, anticancer, and wound-healing agent [11]. AgNPs are also reported for working as catalysts in chemical reactions [12], biolabeling [13], optical receptors [14], and dye degradation. Azo dyes, the major and most versatile class of dyes used in food, paper, and textile industries, are always been a concern for their detrimental effects on the environment. Several physicochemical methods such as adsorption, chemical treatment, and ion-pair extractions have been adopted for the removal of these dyes [15, 16]. The high costs and generation of large amounts of sludge during these processes are the major drawbacks. To overcome these problems, researchers are adopting biological methods of remediation owing to their eco-friendly and green nature [17–19]. Nano-bioremediation is an upcoming technology developed to enhance the existing bioremediation processes.

To fulfill the demands of the increasing population, the industrial revolution has provided better solutions to the way of living. However, it also has its own consequences like increasing pollution and also poses a threat to the environment. Fermentation is one of the industrial operations which, after extracting the desired product, generate a huge amount of waste that is rich in metabolites such as proteins, enzymes, etc. [20]. These wastes usually are not utilized further. In the previous studies, our desired metabolite (arginase), which was produced intracellularly from a mutant *B. licheniformis* M09 by fermentation technology, was extracted from the cell through the downstream process [21]. The scale-up studies of bacterial arginase production led to the generation of liters of the cell-free supernatant as a waste. Any biological system that is rich in metabolites such as proteins [20] functions

as a reducing agent (enzymatic reduction) and, hence, can be explored for the biosynthesis of nanoparticles. This cell-free supernatant may still contain some inorganic and organic compounds with properties conducive for biosynthesis of AgNPs. Such a complementary process may possibly help valorization of a waste supernatant as well as improve the monetary gains from a fermentation process.

In the current study, we have attempted a green approach for the synthesis of AgNPs by utilizing fermentation supernatant left after harvesting cells for the desired biopolymer. The synthesized AgNPs were then characterized and their capability for photocatalytic degradation of methylene blue (azo dye) was evaluated. Furthermore, these AgNPs were also investigated for their antimicrobial activity and cytotoxicity potential against human breast adenocarcinoma cells (MCF-7).

Materials and methods

Materials

All the chemicals used in the study were procured from Hi-Media Ltd, Mumbai. Agar, beef extract, silver nitrate, peptone, yeast extract, manganese chloride, glucose, arginine, sodium chloride, and other media components used were of analytical grade.

Methods

Bacterial strain and its maintenance

The pure culture of *Bacillus licheniformis* (NRS-1264) was procured from Agricultural Research Service (USDA Agricultural Research Service, Salinas, California, USA). The strain was successfully mutagenized for the improved production of arginase and its production media were optimized in the previous studies [21]. The mutant strain, i.e., *B. licheniformis* M09, was further employed for the synthesis of AgNPs. The slants were maintained on optimized media at 4 °C for regular use and subcultured after every 30 days to maintain its potency.

Inoculum and fermentation

The seed (nutrient broth) medium of *B. licheniformis* M09 was inoculated with loopful of cells from previously grown cells from nutrient agar slant. The inoculated flasks were incubated at 37 °C, 180 rpm for 18 h and were used as inoculum for further study. This 18 h old seed (3%, 3×10^7 CFU/mL) was inoculated into sterile production medium (50 mL) in 250 mL of Erlenmeyer flasks. The flasks were incubated for 24 h at 37 ± 2 °C, 180 rpm on an incubator shaker. After 24 h fermentation, the batch was harvested and subjected to centrifugation (Beckman Coulter J2-MC, Brea, USA) at 10,000 rpm (12,100*g*) for 15 min to obtain cell-free supernatant.

Synthesis of the silver nanoparticle using the cell-free supernatant

The core idea behind synthesizing AgNPs was to utilize cell-free supernatant, which was, otherwise, a waste, generated in the process of arginase production by fermentation. The synthesis of silver nanoparticle was initiated by adding sterile $AgNO_3$ (1 mM) to the cell-free supernatant (1:1 v/v) as reducing/stabilizing agents in Erlenmeyer flask and incubated for 36 h at room temperature (28 ± 2 °C) under static condition. In addition, control experiments were also carried out by incubating $AgNO_3$ and cell-free supernatant separately and monitored for any color change in samples at room temperature for 36 h. Samples from each flask were withdrawn at a specific time interval and subjected to absorption spectrum analysis using UV–Vis spectrophotometer (Shimadzu UV 1800, Japan) in the range of 200–800 nm. After 36 h, the flasks were harvested and subjected to centrifugation at 10,000 rpm (12,100 g) (Beckman Coulter J2-MC, Brea, USA) for 20 min to recover AgNPs pellet. The obtained pellets were washed repetitively with distilled water (DW) and dried at 50 °C for 24 h. The AgNPs' powder was used for further studies.

Characterization of AgNPs

UV–Vis spectroscopy The UV–Vis absorption spectra of AgNPs, cell-free bacterial supernatant, and silver nitrate solution (1 mM) were recorded using UV–visible spectrophotometer at a scanning range of 300–800 nm, at 0.5 nm resolution.

X-ray diffraction (XRD) analysis Crystalline nature of dried AgNPs powder was detected by X-ray diffractometer (XRD-6000, Shimadzu Corporation, Tokyo, Japan) using CuKα ($\lambda = 1.54056$ Å). The intensities were recorded at 2θ angles from 5°-80°.

Fourier transform infrared spectroscopy (FTIR) analysis FTIR was performed to determine the presence of functional groups responsible for AgNPs synthesis and stability. The dried powdered sample of control supernatant and synthesized AgNPs was mounted on the Bruker–Alpha's Platinum ATR model (Bruker, Massachusetts, USA) and characterized by attenuated total reflection (ATR) mode at 40 ± 4% relative humidity, 25 °C, and 400–4000 cm^{-1} wave number. The number of spectral resolution and scans was set to 4 and 24 cm^{-1}, respectively.

Particle-size analysis and zeta potential The particle size and zeta potential of AgNPs produced by *B. licheniformis* M09 were analyzed by NanoPlus DLS Particulate Systems (Micromeritics Instrument Corporation, GA, USA) to recognize the particle size and surface charge on AgNPs, respectively.

Transmission electron microscopy (TEM) The shape and size of AgNPs were determined with transmission electron microscopy. AgNPs were dispersed in deionized water and were mounted on a copper grid (300 mesh size). The samples were dried under infrared (IR) lamp for 30 min and subjected for TEM analysis (Tecnai G2, F30 electron microscope, Oregon, USA) instrument operated at 300 kV accelerating voltage.

Applications of biosynthesized AgNPs

Photocatalytic degradation of methylene blue (MB) dye The biosynthesized AgNPs were used for photocatalytic degradation of MB dye ($\lambda_{max} = 660$ nm) under visible light irradiation at a temperature ($T = 25$ °C). In this study, mercury vapor lamp of 400 W enclosed by quartz cylindrical jacket with UV cut-off filter liquid solution was used to obtain the visible light of wavelength ≥ 400 nm. The photodegradation study was carried out by dispersing 20 mg of AgNPs in 100 mL of MB dye solution (10 mg/L) in a Pyrex glass beaker. To ensure constant dispersion of AgNPs in the MB dye solution, the mixture was allowed to stir continuously (200 rpm) for 30 min in dark and then subjected to irradiation under the visible light. The MB solution without AgNPs was also tested under identical condition as a control. The degradation of MB dye solution was investigated by withdrawing an aliquot of 2 mL solution from the beaker at a specific time interval. The samples were centrifuged at 10,000 rpm (12,100*g*) (Beckman Coulter J2-MC, Brea, USA) for 20 min and obtained supernatant was analyzed using UV–Vis spectrophotometer in the wavelength range of 300–800 nm. The percent degradation of dye was calculated using the following equation:

$$\text{Dye degradation } (\%) = \left(\frac{C_0 - C_t}{C_0}\right) \times 100, \quad (1)$$

where C_0 is the initial concentration of MB dye solution and C_t is the concentration of the dye solution after time '*t*'.

Antibacterial activity of silver nanoparticles The antibacterial activity of AgNPs synthesized from the cell-free supernatant was assayed against selected pathogenic microorganisms including Gram-positive (*Bacillus subtilis* subsp. spizizenii ATCC 6633, *Staphylococcus aureus* ATCC 6538) and Gram-negative bacteria (*Escherichia coli* ATCC 25922 and *Pseudomonas aeruginosa* ATCC 10145) using well-diffusion and broth dilution methods.

Well-diffusion method Agar well diffusion was used to evaluate the antibacterial activity of synthesized AgNPs against the above-mentioned organisms. Each strain was spread homogeneously onto the Muller–Hinton agar plates using sterile glass spreader and wells (10 mm) were made in the plates using a sterile cork borer. Different concentrations of AgNPs, viz., 15, 45, and 90 µg/mL, were poured into each well and incubated for 24 h at 30 °C. Inhibition zone was measured after 24 h of incubation.

Broth dilution method The above-mentioned strains were grown in Luria–Bertani broth at 37 °C for 24 h and were serially diluted with fresh sterile LB medium to get an initial absorbance of 0.05 at 600 nm. The 50 µL of AgNPs solution of different concentrations (15, 45, and 90 µg/mL) were added into wells of a 96-well microplate containing 200 µL of fresh sterile LB medium (three replicates), and then, 20 µL of bacterial cell suspension was inoculated in each well followed by incubation for 24 h at 30 °C. The LB broth was used as a control. After 24 h of incubation, absorbance was measured using 96-well microplate reader (µQuant spectrophotometer, BioTek Instruments Pvt Ltd, Mumbai, India) to assess the effect of AgNPs on the growth of studied bacterial strains.

In vitro anticancer/cytotoxicity assay The MTT assay was employed to evaluate anticancer activity/cytotoxicity. Human breast adenocarcinoma cells (MCF-7) were used to investigate the anticancer activity of AgNPs. In brief, 0.1 million MCF-7 cells were seeded in 96-well plate and incubated overnight at 37 °C in 5% CO_2. Furthermore, the cells were treated with different dilutions (5–100 µg/mL) of AgNPs and incubated for 24 h at 37 °C in 5% CO_2. On completion of 24 h, the sample-treated cells were incubated with 10 µL of 5 mg/mL 3-(4,5-dimethyl-1,3-thiazol-2-yl)-2,5-diphenyl-2H-tetrazol-3-ium bromide (MTT) reagent for 4 h. The medium with MTT was then removed and the formed formazan crystals were solubilised using dimethyl sulfoxide (DMSO). The subsequent product concentration was measured by spectrophotometry at 580 nm using microplate reader. The experiments were done in triplicates and cell viability percentage was calculated with respect to control cells incubated without AgNPs treatment using the following equation:

$$\text{Cell viability } (\%) = \left(\frac{\text{OD}_{\text{treated cell}}}{\text{OD}_{\text{untreated cell (control)}}}\right) \times 100. \quad (2)$$

Statistical analysis

All determinations were performed in triplicates and the values were stated as the mean ± standard deviation of three determinations. Analysis of variance (ANOVA) and multiple range Duncan's test were employed using IBM SPSS Statistics 23 software to arbitrate the statistical significance of the differences between the means ($p \leq 0.05$).

Results and discussion

AgNPs synthesis using the cell-free supernatant

The AgNPs synthesis was confirmed by visual observation and UV–visible spectroscopy (Fig. 1). The gradual change in color of the reaction mixture ($AgNO_3$ + cell-free supernatant) with time from pale yellow to dark brown (inset of the figure) indicates the formation of AgNPs [22]. The characteristic absorption peak of AgNPs was observed at around 430 nm and a steady increase in its intensity with reaction time was also perceived. There were no significant color changes observed in control flask containing only $AgNO_3$ solution and cell-free supernatant till 36 h of incubation. Comparable results were reported by Jeevan et al. [23] for AgNPs formation from the supernatant of *P. aeruginosa* culture for 72 h.

Characterization of synthesized silver nanoparticles

XRD analysis

The XRD analysis results showed the clear peaks of cubic phase at 37.94° (1 1 1), 44.35° (2 0 0), 64.51° (2 2 0), and 77.21° (3 1 1) with interlayer spacing $d = 0.236$ nm, $d = 0.204$ nm, $d = 0.144$ nm, and $d = 0.124$ nm, respectively (Fig. 2a). All of these peaks were indexed to the standard cubic phase of AgNPs. Comparison of the XRD spectrum with the standard confirmed the crystalline nature of AgNPs. Similar results were reported by Philip et al. [24] and Jeevan et al. [23] using *Fusarium oxysporum* and *Pseudomonas aeruginosa*, respectively.

FTIR spectroscopy

To determine the possible bio-reducing functional groups involved in the reduction of Ag^+ ions and stabilization of AgNPs, FTIR analysis of control supernatant and AgNPs was performed and the results are presented in Fig. 2a, b, respectively. The spectra showed strong bands at 3286 cm^{-1}, 2108 cm^{-1}, 1638 cm^{-1}, 1560 cm^{-1}, 1414 cm^{-1}, 1261 cm^{-1}, 1072 cm^{-1}, and 707 cm^{-1} for control supernatant and 3447 cm^{-1}, 2122 cm^{-1}, 1639 cm^{-1}, 1555 cm^{-1}, 1414 cm^{-1}, 1098 cm^{-1}, 1021 cm^{-1}, and 658 cm^{-1} for synthesized AgNPs. The bands at 3400–3500 cm^{-1} indicate amino

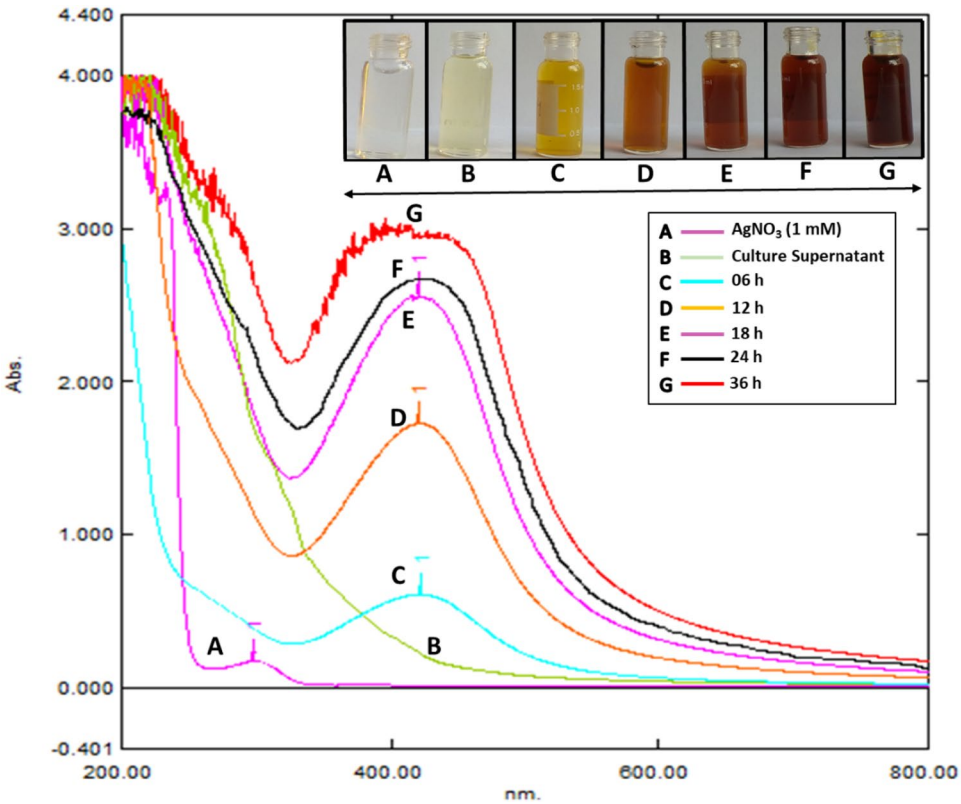

Fig. 1 UV–visible absorption spectrum of the reacting mixture at different time intervals. The inset of the figure shows a sequential visual change in the color of reaction from pale yellow to dark brown depicting the synthesis of AgNPs

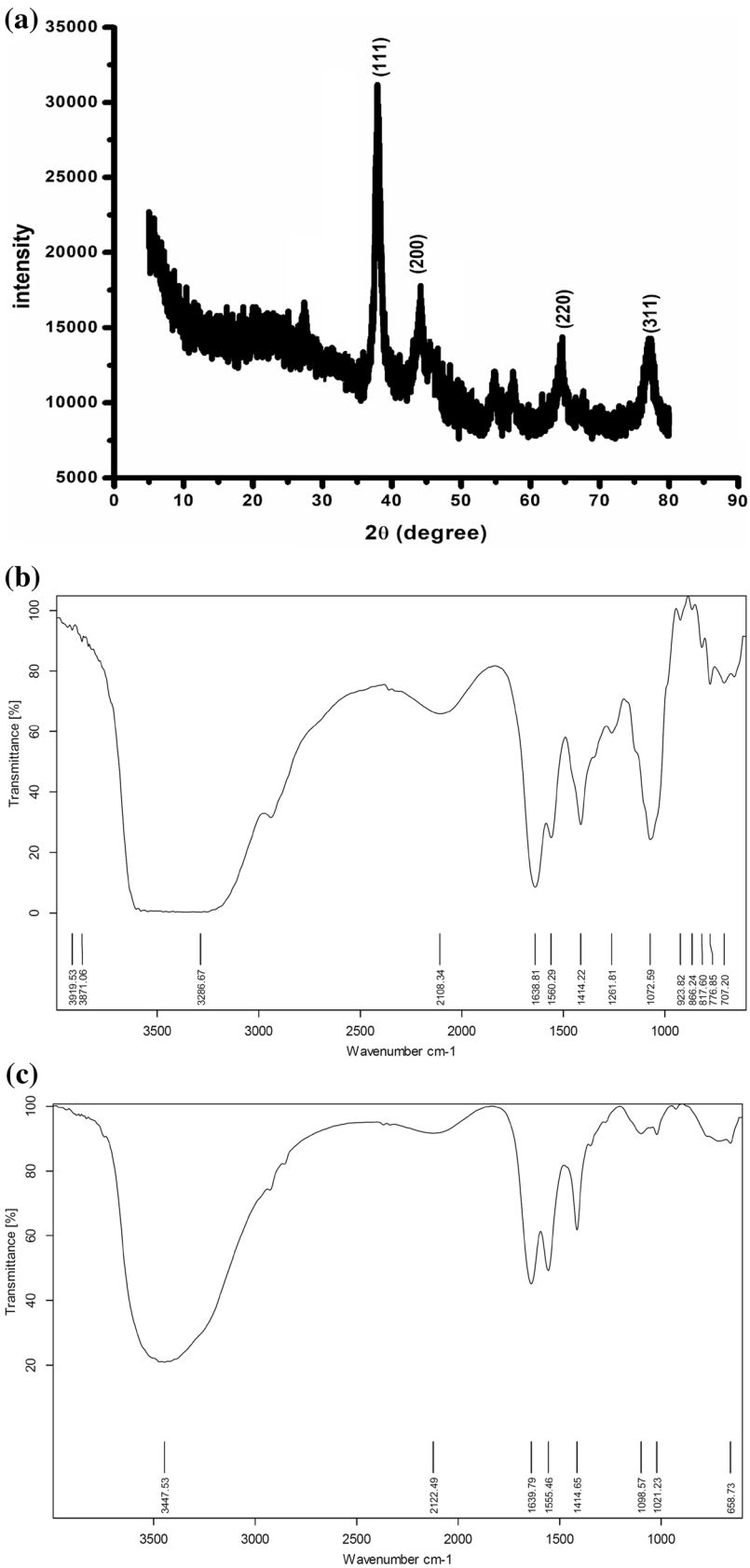

Fig. 2 **a** X-ray diffraction curve of AgNPs. **b** FTIR spectrum of supernatant (control), and **c** AgNPs, synthesized after 72 h of incubation using *B. licheniformis* M09 supernatant

group stretching and antisymmetric stretching of C–H bond in methyl group of protein or polysaccharide, respectively [26], while NH bending of primary alkalamides and stretching of C–N bonds in C = N bond of amide-II region can be confirmed by functional peaks at 1700–1550 cm^{-1} [27]. The distinctive peaks at 1414 cm^{-1} indicate O–H bending, while 1098 and 1021 cm^{-1} revealed the C–O stretching (Fig. 2b). The band at the peak detected at 707 cm^{-1} is allocated to bounded amine groups (–NH) of supernatant which is shifted to 658 cm^{-1} after the reduction of silver nitrate. It is well recognized that biological components having these functional groups interact with metal salts and leads to the reduction process [28]. These peaks clearly suggested the involvement of carboxylic and amine groups in reducing silver salts for the synthesis of AgNPs [29, 30].

Particle-size analysis and zeta potential

Dynamic light scattering (DLS) and zeta potential were employed to determine the size of the particles and their potential stability in the colloidal suspension. Figure 3a exhibits the particle-size distribution of AgNPs synthesized by *B. licheniformis* M09. The mean particle hydrodynamic size of the AgNPs in aqueous solution was found to be 20 nm and zeta potential of − 11.37 ± 0.04 mV (Fig. 3b). The present values of zeta potential confirmed the moderate stability of AgNPs [31]. Kalpana and Lee [32] reported similar results using supernatant of *K. pneumoniae* for the AgNPs synthesis, in which the particles range in size from 15 to 37 nm with an average size of 22 nm.

Transmission electron microscopy (TEM)

The transmission electron microscopy was performed to understand the morphology and microstructure of the AgNPs. Figure 4a shows the low magnification TEM image which revealed the average size of AgNPs is around 10–30 nm. The high-resolution (HR) TEM in Fig. 4b confirms that the synthesized AgNPs are mono-dispersed and spherical in shape. Figure 4c represents the fast Fourier

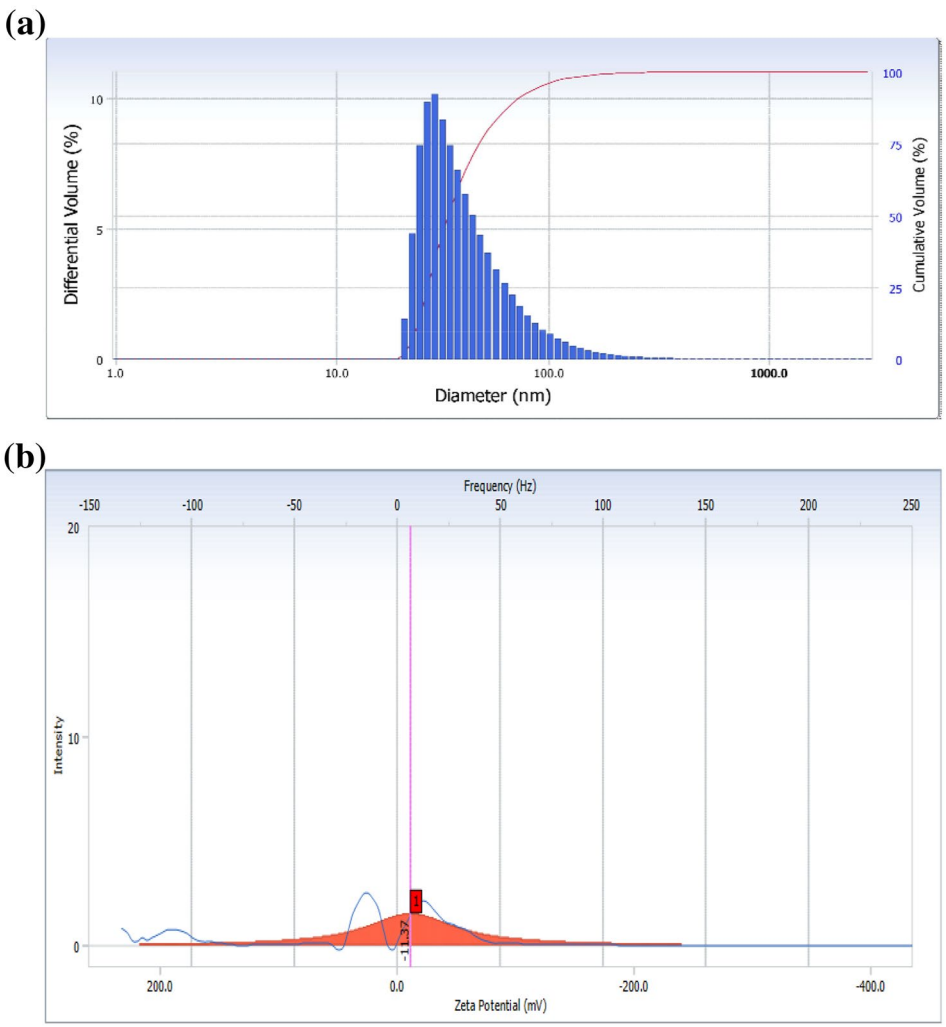

Fig. 3 **a** Particle-size histogram showing the distribution and **b** zeta-potential analysis of AgNPs synthesized using *B. licheniformis* M09

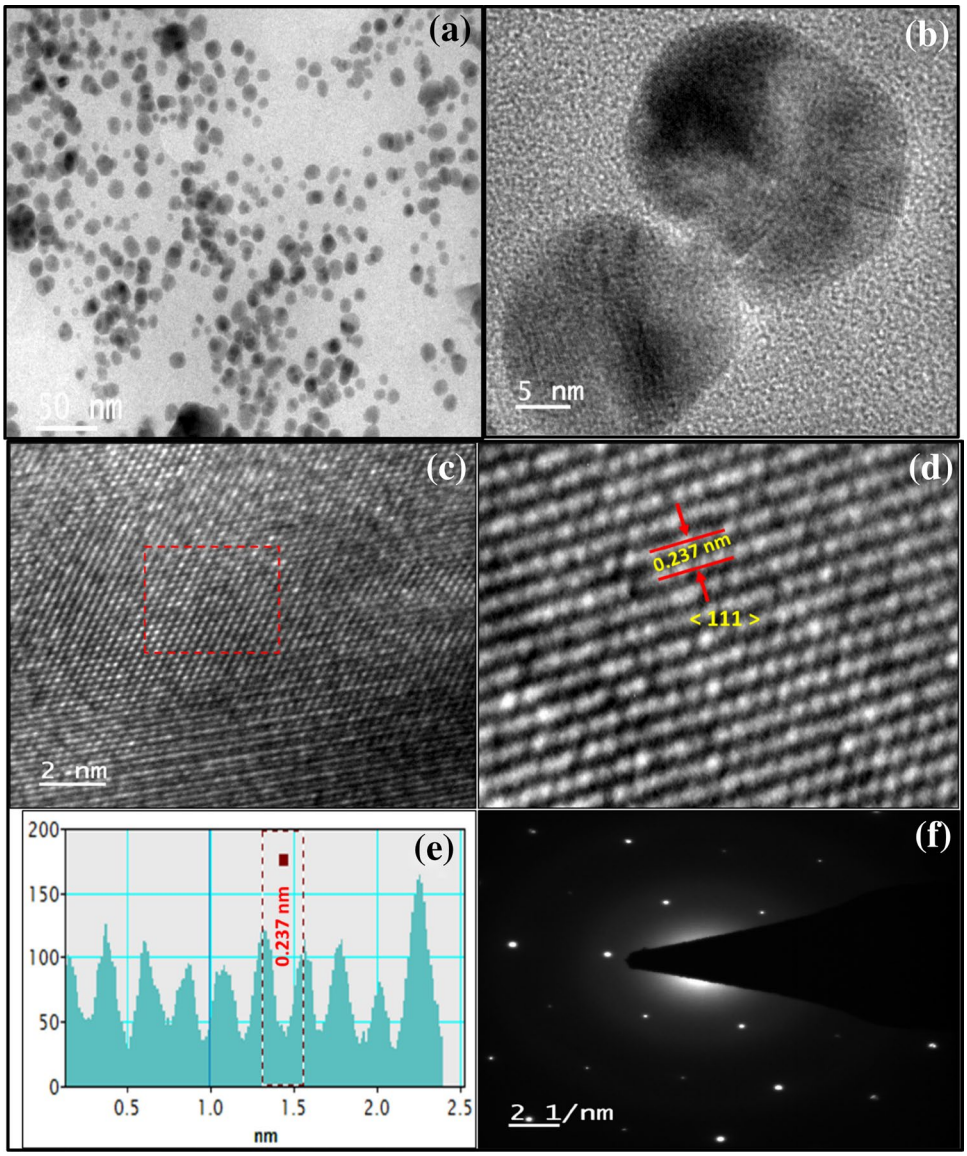

Fig. 4 **a** TEM images of AgNPs. **b** HR-TEM images of representative AgNPs. **c** HR-TEM image showing crystal lattice fringes. **d** Integrated image from the FFT plot; **e** line spectra showing inter-planer spacing and **f** selected area electron diffraction (SAED) pattern

transform (FFT) view of the HR-TEM image of AgNPs. Figure 4d shows the inverse FFT of crystalline AgNPs with an interlayer spacing of $d = 0.237$ nm which corresponds to (111) plane. Figure 4e shows the line profile spectra of crystalline AgNPs with an inter-planer spacing of $d = 0.237$ nm. The face-centered cubic (FCC) crystalline structure of AgNPs was validated by the selected area electron diffraction (SAED) pattern (Fig. 4f) in conjunction with XRD studies.

Applications of biosynthesized AgNPs

Photocatalytic degradation of methylene blue (MB) dye

The photocatalytic property of biosynthesized AgNPs for MB dye degradation was studied under visible light irradiation and the results are presented in Fig. 5a. The deep blue color of dye (0 min) changed to light blue (105 min) and then colorless after 180 min of irradiation with AgNPs under visible light (inset of Fig. 5a). The distinct absorption peak (at 664 nm) of MB solution decreased with exposure time and was approaching the baseline after 180 min. The dye degradation was found to be 94% after 180 min of light exposure (Fig. 5b). Similar kinds of results were reported by Vanaja et al. [33] where the MB maximum degradation was achieved after 72 h using AgNPs synthesized from *Morinda tinctoria*. Figure 5c shows the kinetic curves for photocatalytic degradation of MB by plotting C/C_0 v/s time, where C is the final concentration and C_0 is the initial concentration obtained as a function of irradiation and reveals the excellent photocatalytic efficiency. In Fig. 5d, kinetic curves demonstrate the pseudo-first-order linear form $\ln (C/C_0) = kt$, where

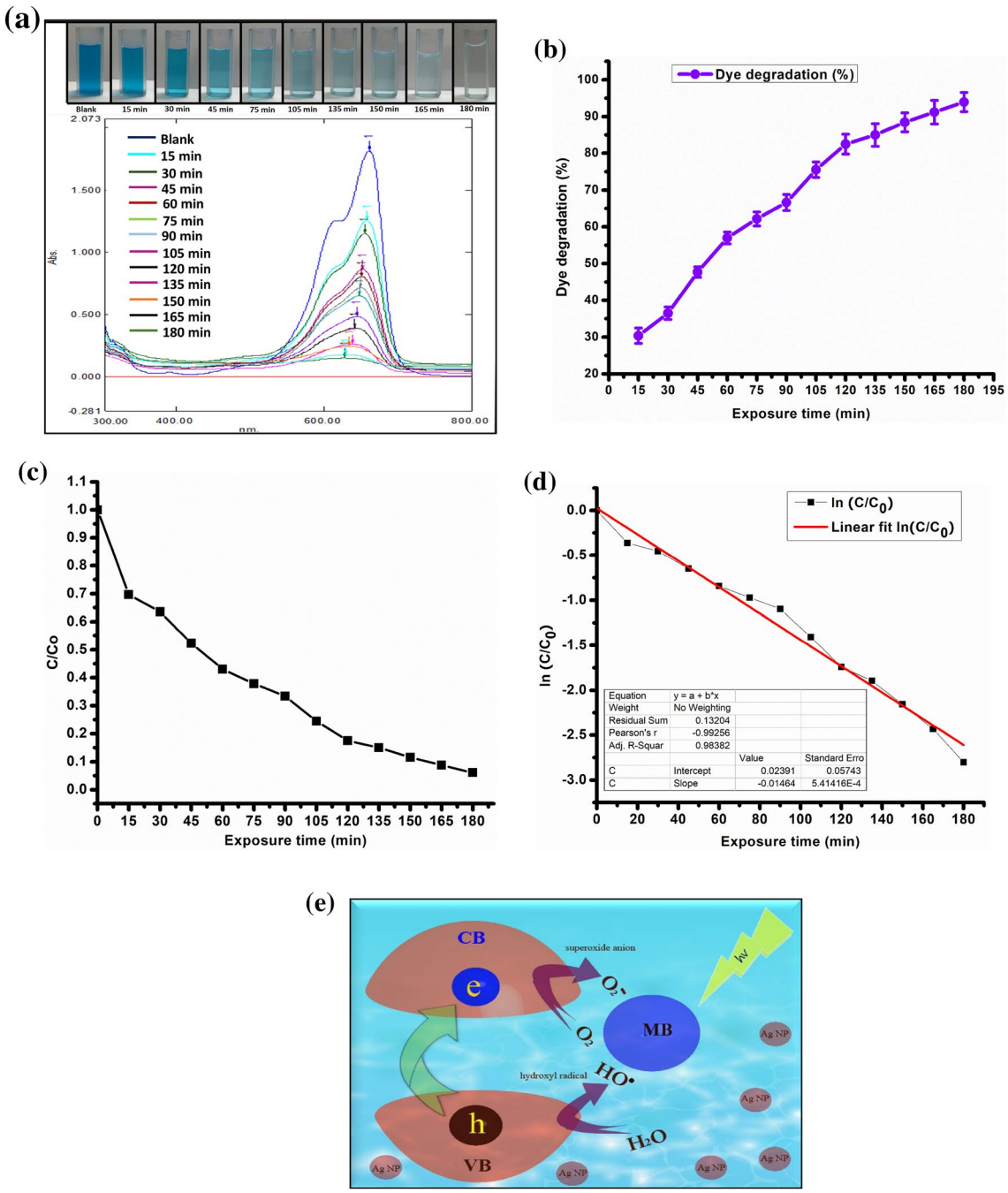

Fig. 5 **a** UV–visible absorption spectrum indicates the photocatalytic degradation of methylene blue dye at different time intervals. The inset of the figure shows gradual visual observation of the color change of dye from blue to colorless. **b** Line graph showing MB dye degradation % at the different time interval of visible light exposure. **c** Kinetic curves for degradation of MB dye. **d** Kinetic fits (ln (C/C_0) vs. time) curve for degradation of MB dye. **e** Schematic illustration of putative mechanism leads to photocatalytic degradation of methylene blue dye using biosynthesized AgNPs

k and *t* are apparent rate constants [34, 35]. However, in the present study, the MB solution showed a significant degradation of dye with an exposure period of 180 min. Figure 5e exemplifies the graphical representation of the putative mechanism which leads to photocatalytic degradation of MB dye using biosynthesized AgNPs. When AgNPs is exposed to visible light irradiation, a photon energy ($h\nu$) equal or greater than the bandgap excites the electron (e^-) from filled valence band (VB) to the empty conduction band (CB) and leaving hole (h^+) behind in the valence band [36]. The hole

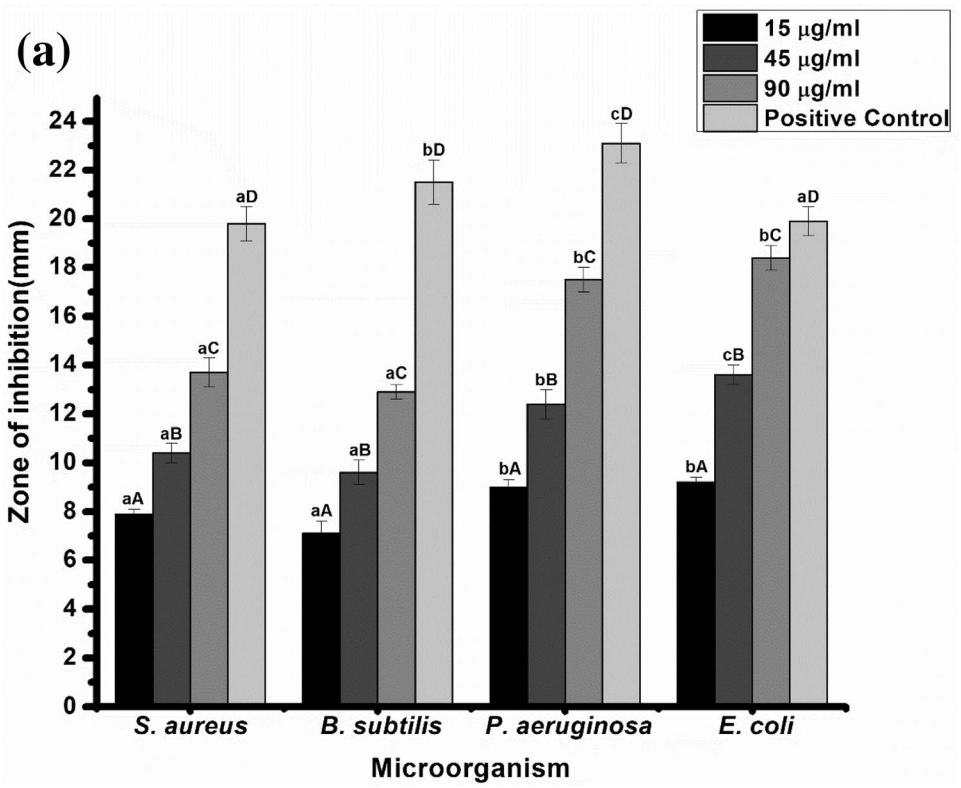

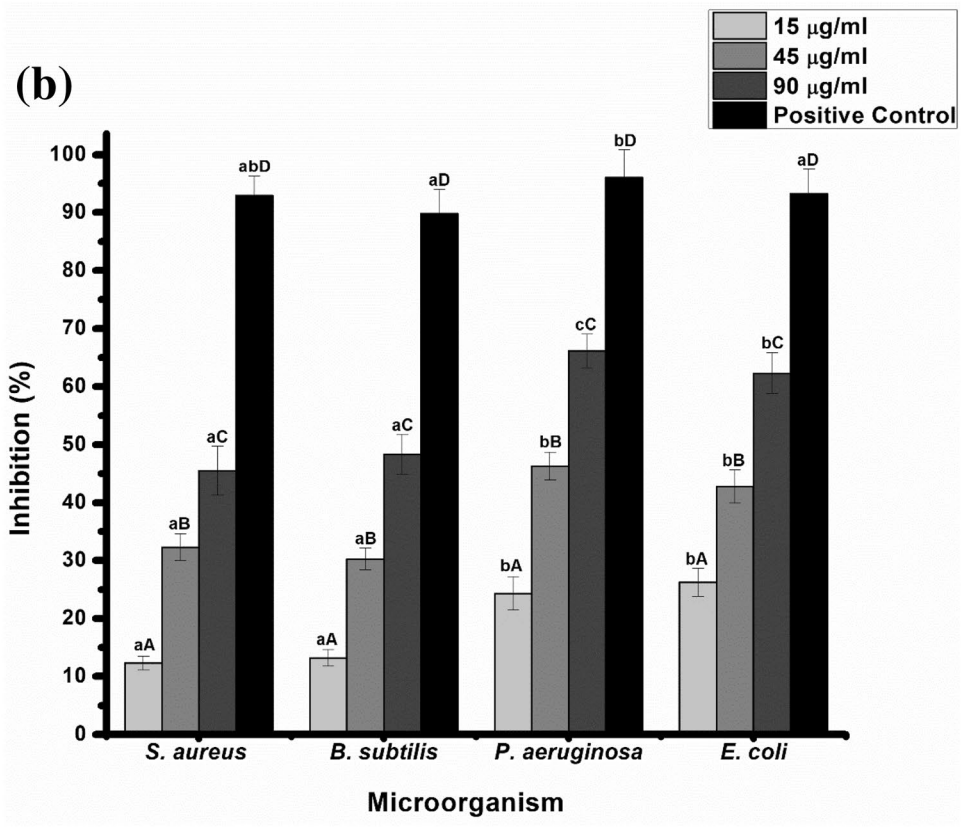

Fig. 6 Graphical representation of antibacterial activity of biosynthesized AgNPs with **a** size of zone of inhibition using well-diffusion method and **b** percent inhibition of bacterial growth using broth dilution method, against four tested bacteria: (1) *Staphylococcus aureus*, (2) *Bacillus subtilis*, (3) *Pseudomonas aeruginosa*, and (4) *Escherichia coli*

in the valence band reacts with water molecule (H_2O) adsorb on the surface of AgNPs to produce hydroxyl-free radical ($OH^{\cdot}$) which is powerful oxidizing agent and electron in the conduction band react with O_2 to produce superoxide ions O_2^- which is a strong-reducing agent. Both the oxidizing and reducing agents are active reagents to decompose dye into simpler organic molecules adsorb on the surface of AgNPs [37–39]. Therefore, for the degradation of MB under visible light irradiation, the biosynthesized AgNPs may act as effective photocatalyst [33, 40].

Antibacterial activity of silver nanoparticles

The prominent zones of inhibition against both Gram-positive and Gram-negative bacteria were observed using AgNPs. The diameter of zone of inhibition was found to increase with an increase in the concentration of AgNPs showing more noticeable effect towards Gram-negative organisms (Fig. 6a). Zone of inhibition assay, thus, provided a preliminary information about AgNPs' antibacterial activity against selected bacteria. Broth dilution assay was further performed to evaluate percent growth inhibition of selected bacteria at various concentrations of AgNPs (Fig. 6b). The results revealed that the bacterial growth was inhibited by AgNPs in a dose-dependent manner. The growth of *S. aureus, B. subtilis, P. aeruginosa*, and *E. coli* was inhibited by 12, 13, 24, and 26% at a lower concentration (15 µg/mL) of AgNPs, and by 45, 48, 66, and 62% at higher concentration (90 µg/mL), respectively. Since AgNPs synthesized using *B. licheniformis* M09 are of smaller in size, they probably have better-penetrating abilities through cell wall resulted in enhanced cidal effect against Gram-negative bacteria. Though the detailed mechanism behind the efficacy of silver nanoparticles as an antibacterial agent is still unclear, it might be due to its penetration into the cell membrane by adhesion and further interaction with genetic material leading to the inhibition of replication process by altering the protein involved in the duplication of DNA and cellular metabolism [41].

In vitro anticancer/cytotoxicity

In this study, the cytotoxicity of biogenic AgNPs was tested against MCF-7 cell line by MTT assay and percentage cell viability was investigated (Fig. 7). The MTT assay is a widely accepted method which relies on the fact that the reduction of MTT to purple formazan is proportionate to the level of energy metabolism in the cells. Hence, the spectrophotometrical measurement of dye intensity is directly related to the number of viable cells. The proliferation of cancer cells (MCF-7) was found to be inhibited in a dose-dependent manner when treated with varying concentrations of AgNPs. The green-synthesized AgNPs did not show a substantial effect on cell viability at lower concentrations. However, the cytotoxic effect was observed to increase with increase in concentrations of AgNPs. The cell growth was inhibited by 3, 9, 20, 44, 69, and 90% with the administration of 5, 10, 25, 50, 75, and 100 µg/mL of AgNPs, respectively. Following the observations of cytotoxicity induced by AgNPs on MCF-7 cells resulted in the inhibitory concentration (IC_{50}) value of 56.25 µg/mL. The results suggest that AgNPs possess strong cytotoxic ability against MCF-7 cells and our findings go well in agreement with the results reported in the earlier studies [42, 43].

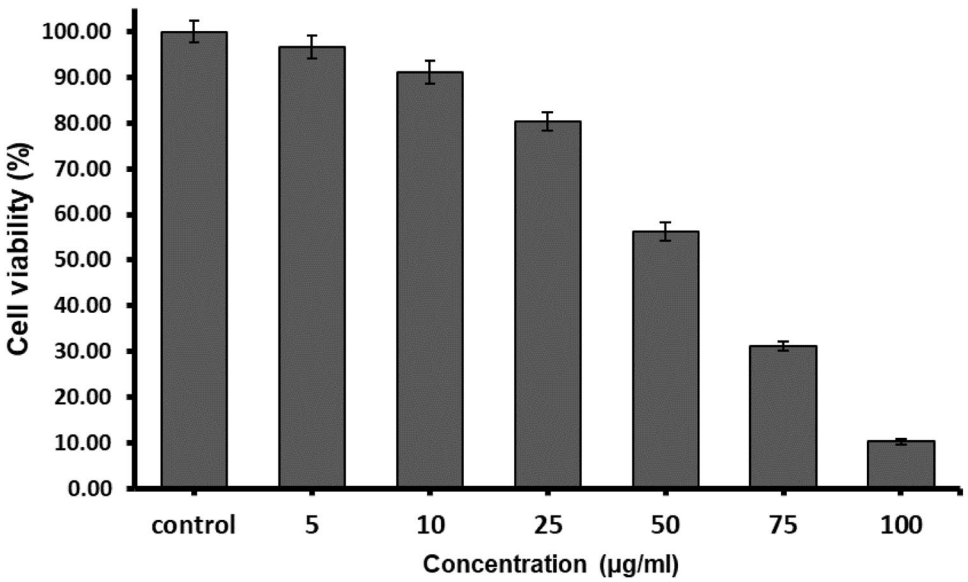

Fig. 7 Graphical representation of in vitro cytotoxicity effect of biosynthesized AgNPs on human breast adenocarcinoma cells (MCF-7)

Conclusion

The present research demonstrated an efficient green synthesis approach for the synthesis of AgNPs from waste supernatant generated after separating *B. licheniformis* M09 cells in fermentative arginase production. The biosynthesized AgNPs efficiently degraded MB dye with visible light irradiation and also proved to be an excellent antimicrobial as well as an anticancer agent. The current work suggests new approaches on similar lines by utilizing the other fermentation wastes, possibly rich in reducing agents for the synthesis of various nanoparticles. The outcomes of this study recommend that, apart from being simple, cost-effective and compatible, AgNPs synthesized by a facile method from waste supernatant are an efficient way for effluent treatment, ecological health, and environmental bioremediation. These biosynthesized AgNPs can also be explored for application in the field of pharmaceutics and food preservation.

Acknowledgements Authors are grateful to the University Grants Commission, India, for the financial support provided for this research.

Compliance with ethical standards

Conflict of interest The authors declare that they have no conflict of interest towards this research.

Ethical approval This article does not include any studies with human participants or animals performed by any authors.

References

1. Vidor FF, Meyers T, Müller K et al (2017) Inverter circuits on freestanding flexible substrate using ZnO nanoparticles for cost-efficient electronics. Solid State Electron 137:16–21. https://doi.org/10.1016/j.sse.2017.07.011
2. Gittins DI, Bethell D, Nichols RJ, Schiffrin DJ (2000) Diode-like electron transfer across nanostructured films containing a redox ligand. J Mater Chem 10:79–83. https://doi.org/10.1039/a902960e
3. Crooks R, Lemon B III, Sun L et al (2001) Dendrimer-encapsulated metals and semiconductors: synthesis, characterization, and applications. Top Curr Chem 212:81–135
4. Chen S, Fu P, Yin B et al (2011) Immobilizing Pt nanoparticles and chitosan hybrid film on polyaniline nanofibers membrane for an amperometric hydrogen peroxide biosensor. Bioprocess Biosyst Eng 34:711–719. https://doi.org/10.1007/s00449-011-0520-4
5. Ladole MR, Nair RR, Bhutada YD et al (2018) Synergistic effect of ultrasonication and co-immobilized enzymes on tomato peels for lycopene extraction. Ultrason Sonochem. https://doi.org/10.1016/j.ultsonch.2018.06.013
6. Muley AB, Thorat AS, Singhal RS, Babu KH (2018) A tri-enzyme co-immobilized magnetic complex: Process details, kinetics, thermodynamics and applications. Int J Biol Macromol 118:1781–1795. https://doi.org/10.1016/j.ijbiomac.2018.07.022
7. Singh M, Chandrasekaran N, Mukherjee A et al (2014) Cancerous cell targeting and destruction using pH stabilized amperometric bioconjugated gold nanoparticles from marine macroalgae, *Padina gymnospora*. Bioprocess Biosyst Eng 37:1859–1869. https://doi.org/10.1007/s00449-014-1160-2
8. Jacob SJP, Prasad VLS, Sivasankar S, Muralidharan P (2017) Biosynthesis of silver nanoparticles using dried fruit extract of *Ficus carica*—screening for its anticancer activity and toxicity in animal models. Food Chem Toxicol 109:951–956. https://doi.org/10.1016/j.fct.2017.03.066
9. Konishi Y, Ohno K, Saitoh N et al (2007) Bioreductive deposition of platinum nanoparticles on the bacterium Shewanella algae. J Biotechnol 128:648–653. https://doi.org/10.1016/j.jbiotec.2006.11.014
10. Willner I, Baron R, Willner B (2006) Growing metal nanoparticles by enzymes. Adv Mater 18:1109–1120. https://doi.org/10.1002/adma.200501865
11. Firdhouse MJ, Lalitha P (2015) Biosynthesis of silver nanoparticles and its applications. J Nanotechnol. https://doi.org/10.1155/2015/829526
12. Kumar A, Mandal S, Selvakannan PR et al (2003) Investigation into the interaction between surface-bound alkylamines and gold nanoparticles. Langmuir 19:6277–6282. https://doi.org/10.1021/la034209c
13. Malvindi MA, Di Corato R, Curcio A et al (2011) Multiple functionalization of fluorescent nanoparticles for specific biolabeling and drug delivery of dopamine. Nanoscale 3:5110–5119. https://doi.org/10.1039/c1nr10797f
14. Parashar UK, Saxena PS (2009) Bioinspired synthesis of silver nanoparticles. J Nanomater 4:159–166
15. Paul M, Pal N, Bhaumik A (2012) Selective adsorption and release of cationic organic dye molecules on mesoporous borosilicates. Mater Sci Eng C 32:1461–1468. https://doi.org/10.1016/j.msec.2012.04.026
16. Pal J, Deb MK (2014) Efficient adsorption of congo red dye from aqueous solution using green synthesized coinage nanoparticles coated activated carbon beads. Appl Nanosci 4:967–978. https://doi.org/10.1007/s13204-013-0277-y
17. Rosales E, Pérez-Paz A, Vázquez X et al (2012) Isolation of novel benzo[a]anthracene-degrading microorganisms and continuous bioremediation in an expanded-bed bioreactor. Bioprocess Biosyst Eng 35:851–855. https://doi.org/10.1007/s00449-011-0669-x
18. Gadd GM (2004) Microbial influence on metal mobility and application for bioremediation. Geoderma 122:109–119. https://doi.org/10.1016/j.geoderma.2004.01.002
19. Almeida É, De Oliveira D, Hotza D (2017) Characterization of silver nanoparticles produced by biosynthesis mediated by *Fusarium oxysporum* under different processing conditions. Bioprocess Biosyst Eng 40:1291–1303. https://doi.org/10.1007/s00449-017-1788-9
20. Jenzsch M, Simutis R, Eisbrenner G et al (2006) Estimation of biomass concentrations in fermentation processes for recombinant protein production. Bioprocess Biosyst Eng 29:19–27. https://doi.org/10.1007/s00449-006-0051-6
21. Momin B, Chakraborty S, Annapure U (2018) Investigation of the cell disruption methods for maximizing the extraction of arginase from mutant *Bacillus licheniformis* (M09) using statistical approach. Korean J Chem Eng 35:1–12. https://doi.org/10.1007/s11814-018-0107-8
22. Quinteros MA, Aiassa Martínez IM, Dalmasso PR, Páez PL (2016) Silver Nanoparticles: Biosynthesis using an ATCC reference strain of *Pseudomonas aeruginosa* and activity as broad spectrum clinical antibacterial agents. Int J Biomater. https://doi.org/10.1155/2016/5971047
23. Jeevan P, Ramya K, Rena AE (2012) Extracellular biosynthesis of silver nanoparticles by culture supernatant of *Pseudomonas aeruginosa*. Indian J Biotechnol 11:72–76

24. Philip D (2009) Biosynthesis of Au, Ag and Au-Ag nanoparticles using edible mushroom extract. Spectrochim Acta - Part A Mol Biomol Spectrosc 73:374–381. https://doi.org/10.1016/j.saa.2009.02.037
25. Huang J, Li Q, Sun D et al (2007) Biosynthesis of silver and gold nanoparticles by novel sundried *Cinnamomum camphora* leaf. Nanotechnology. https://doi.org/10.1088/0957-4484/18/10/105104
26. Sanghi R, Verma P (2009) Biomimetic synthesis and characterisation of protein capped silver nanoparticles. Bioresour Technol 100:501–504. https://doi.org/10.1016/j.biortech.2008.05.048
27. Muley AB, Chaudhari SA, Mulchandani KH, Singhal RS (2018) Extraction and characterization of chitosan from prawn shell waste and its conjugation with cutinase for enhanced thermo-stability. Int J Biol Macromol 111:1047–1058. https://doi.org/10.1016/j.ijbiomac.2018.01.115
28. Ajitha B, Kumar YA, Reddy PS (2014) Molecular and Biomolecular Spectroscopy Biosynthesis of silver nanoparticles using *Plectranthus amboinicus* leaf extract and its antimicrobial activity. Spectrochim ACTA Part A Mol Biomol Spectrosc 128:257–262. https://doi.org/10.1016/j.saa.2014.02.105
29. Kishore Y, Sujit M, Behera K (2014) Biosynthesis, characterization and antimicrobial activity of silver nanoparticles by *Streptomyces* sp. SS2:2263–2269. https://doi.org/10.1007/s00449-014-1205-6
30. Vanaja M, Gnanajobitha G, Paulkumar K et al (2013) Phytosynthesis of silver nanoparticles by *Cissus quadrangularis*: Influence of physicochemical factors. J Nanostruct Chem 3:17. https://doi.org/10.1186/2193-8865-3-17
31. Drzewiecka WW, Gaikwad S, Laskowski D, Niedojadło HD et al (2014) Novel approach towards synthesis of silver nanoparticles from *Myxococcus virescens* and their lethality on pathogenic bacterial cells. J Biotechnol Bioeng 1:1–7
32. Kalpana D, Lee YS (2013) Synthesis and characterization of bactericidal silver nanoparticles using cultural filtrate of simulated microgravity grown *Klebsiella pneumoniae*. Enzyme Microb Technol 52:151–156. https://doi.org/10.1016/j.enzmictec.2012.12.006
33. Vanaja M, Paulkumar K, Baburaja M et al (2014) Degradation of methylene blue using biologically synthesized silver nanoparticles. Bioinorg Chem Appl 2014:1–8
34. Zhu Y, Dan Y (2010) Photocatalytic activity of poly(3-hexylthiophene)/titanium dioxide composites for degrading methyl orange. Sol Energy Mater Sol Cells 94:1658–1664. https://doi.org/10.1016/j.solmat.2010.05.025
35. Liu Y, Xie S, Li H, Wang X (2014) A highly efficient sunlight driven ZnO nanosheet photocatalyst: synergetic effect of *p*-doping and MoS2 atomic layer loading. ChemCatChem 6:2522–2526. https://doi.org/10.1002/cctc.201402191
36. Yu L, Xi J, Li M-D et al (2012) The degradation mechanism of methyl orange under photo-catalysis of TiO_2. Phys Chem Chem Phys 14:3589. https://doi.org/10.1039/c2cp23226j
37. Houas A (2001) Photocatalytic degradation pathway of methylene blue in water. Appl Catal B Environ 31:145–157. https://doi.org/10.1016/S0926-3373(00)00276-9
38. Ameta A, Ameta R, Ahuja M (2013) Photocatalytic degradation of methylene blue over ferric tungstate. Sci Rev Chem Commun 3:172–180
39. Borase HP, Patil CD, Salunkhe RB et al (2014) Transformation of aromatic dyes using green synthesized silver nanoparticles. Bioprocess Biosyst Eng 37:1695–1705. https://doi.org/10.1007/s00449-014-1142-4
40. Khan AU, Malik N, Khan M et al (2018) Fungi-assisted silver nanoparticle synthesis and their applications. Bioprocess Biosyst Eng. https://doi.org/10.1007/s00449-017-1846-3
41. Lemire JA, Harrison JJ, Turner RJ (2013) Antimicrobial activity of metals: mechanisms, molecular targets and applications. Nat Rev Microbiol 11:371–384. https://doi.org/10.1038/nrmicro3028
42. Sudha A, Jeyakanthan J, Srinivasan P (2017) Resource-efficient technologies green synthesis of silver nanoparticles using *Lippia nodiflora* aerial extract and evaluation of their antioxidant, antibacterial and cytotoxic effects. Resour Technol 3:506–515. https://doi.org/10.1016/j.reffit.2017.07.002
43. Gopinath V, Priyadarshini S, Fai M et al (2017) Biogenic synthesis, characterization of antibacterial silver nanoparticles and its cell cytotoxicity. Arab J Chem 10:1107–1117. https://doi.org/10.1016/j.arabjc.2015.11.011

Affiliations

Bilal Momin[1] · Shakeelur Rahman[2] · Neetu Jha[2] · Uday S. Annapure[1]

✉ Uday S. Annapure
us.annapure@ictmumbai.edu.in

[1] Department of Food Engineering and Technology, Institute of Chemical Technology, Matunga, Mumbai 400019, India

[2] Department of Physics, Institute of Chemical Technology, Matunga, Mumbai 400019, India